A case study analysis of the impact of a new free tropospheric turbulence scheme on the dispersion of an atmospheric tracer

Received: 21 September 2023 | Revised: 5 January 2024 | Accepted: 2 February 2024

DOI: 10.1002/qj.4681

Quarterly Journal of the Royal Meteorological Society RMetS

RESEARCH ARTICLE

A case study analysis of the impact of a new free tropospheric turbulence scheme on the dispersion of an atmospheric tracer

Andrew K. Mirza | **Helen F. Dacre** | **Chun Hay Brian Lo**

Department of Meteorology, Brian Hoskins Building, University of Reading, Reading, United Kingdom

Correspondence
Andrew K. Mirza, Department of Meteorology, Brian Hoskins Building, University of Reading, Whiteknights Campus, Reading, RG6 6ET, United Kingdom.
Email: andrew.mirza@reading.ac.uk

Funding information
Department of Meteorology, University of Reading; Met Office; Natural Environment Research Council, Grant/Award Number: NE/S004505/1

Abstract

Most Lagrangian dispersion models represent free tropospheric turbulence as a homogeneous steady-state process. However, intermittent turbulent mixing in the free troposphere may be a significant source of mixing. We test a new parametrization scheme that represents spatial- and temporal-varying turbulence in the free troposphere in the Met Office's Numerical Atmospheric-dispersion Modelling Environment. We use semi-idealized emissions of radon-222 (^{222}Rn) from rocks and soil in the United Kingdom to evaluate the impact of using a variable free tropospheric turbulence parameterization on the dispersion of ^{222}Rn. We performed two experiments, the first using the existing steady-state scheme and the second using the newly implemented spatio-temporal-varying scheme, for two case periods July 2018 and April 2021. We find that the turbulence in the varying scheme (represented by the vertical velocity variance) can range by two to three orders of magnitude (10^{-4} to 10^{-1} m^2 ·s^{-2}) when compared with the steady-state scheme (10^{-2} m^2 ·s^{-2}). In particular, low-altitude turbulence is enhanced when synoptic conditions are conducive to forming low-level jets. This leads to a greater dispersion in the free troposphere, reducing the mean monthly ^{222}Rn concentration above the boundary layer by 20–40% relative to the steady-state scheme. We conclude that without a space–time-varying free tropospheric turbulence scheme atmospheric dispersion may be significantly underestimated under synoptic conditions that are favourable for low-level jet formation. This underestimation of dispersion may potentially result in inaccurate estimations of local emissions in top-down greenhouse gas inventory studies.

KEYWORDS

air pollution, atmospheric dispersion, free tropospheric turbulence, greenhouse gas emissions, inventory studies, low-level jets, radon tracer

1 | INTRODUCTION

Turbulent mixing in the atmospheric boundary layer is common. The resultant mixing affects the concentration field of pollutants, such as smoke from fires, radioactive material from nuclear accidents, and greenhouse gases. Mixing in turbulent flows and its relationship to the dispersion of pollutants in the atmospheric boundary layer have been widely studied (e.g., Barad (1958); Gifford (1959); Hanna (1981); Mason (1992); Turner (1997); Ott and Ejsing Jørgensen (2002); Jones (2004); Ferrero et al. (2023); and references therein). In the atmosphere above the boundary layer, known as the free troposphere (or the free atmosphere), turbulent mixing occurs in localized, intermittent events. The study of turbulence in the free troposphere and its effect on the dispersion of pollutants has received relatively less attention.

Most numerical dispersion models do not represent this free tropospheric intermittent turbulence and instead assume steady-state conditions for turbulent mixing. This is the case in a range of commonly used dispersion models (Bonadonna et al., 2012). In a review of the latest available documentation for the dispersion models — Ash3D (Schwaiger et al., 2012), FLEXPART (Stohl et al., 2005), HYSPLIT (Draxler & Hess, 1998), JMA-ATM (Saito et al., 2015), MLDP0 (D'Amours et al., 2015), PUFF (Searcy et al., 1998), and Vol-CALPUFF (Barsotti et al., 2008) — we conclude that only HYSPLIT in its Lagrangian mode includes schemes that could represent space–time-varying turbulence in the free troposphere.

Failure to represent this intermittent turbulence could lead to the over- or underestimation of pollutant concentrations in dispersion forecasts (Dacre et al., 2015). Sensitivity studies suggest that poor representation of free tropospheric turbulence is a source of major uncertainty in dispersion simulations (Harvey et al., 2018; Swallow et al., 2017). This article aims to investigate a space- and time-varying free tropospheric turbulence scheme in the UK Met Office's Numerical Atmospheric-dispersion Modelling Environment (NAME) (Jones et al., 2007) and to analyse the synoptic conditions under which turbulence is significantly enhanced or suppressed in the free troposphere. The effect of space- and time-varying turbulence on the mixing of pollutants is illustrated by quantifying differences in Radon-222 (^{222}Rn) concentrations in the free troposphere between simulations using the steady-state turbulence and the new space–time-varying turbulence.

Turbulence in the free troposphere is intermittent, with regions forming sporadically, generating mixing in a localized region, and then decaying. Thus, unlike the boundary layer, there is no significant permanent background field of turbulence in the free troposphere. If the free troposphere is unstable then convection will occur, leading to localized mixing over a large vertical extent of the atmosphere. In a stably stratified free troposphere, the airflow is laminar. The main mechanism for disrupting this laminar flow is turbulence generation from wind shear instability (Ludlam, 1967; Roach, 1970). When the destabilizing effect of wind shear is sufficient to overcome the dampening influence of stability, turbulence will intensify. When turbulent mixing sufficiently weakens the background wind shear, the turbulence will decay and the flow will again become laminar (Miles, 1961). Strong vertical wind shear typically occurs on the edges of localized wind-speed maxima (known as jets). This mechanism of turbulent mixing often occurs in the air that is cloudless and is known as clear-air turbulence (CAT). Thus, CAT is frequently found in the upper troposphere, near midlatitude jet streams; in the midtroposphere, associated with frontal cyclones; and in the lower troposphere, near low-level jets (LLJs).

We focus on LLJs in this article, as they are most likely to influence near-surface air concentrations and long-range transport of pollutants; for example, ozone, mineral dust, and particulates (Wei et al., 2023). There are several types of LLJ. Nocturnal LLJs occur at night and are due to inertial oscillations when the air at the top of the daytime boundary layer becomes decoupled from the air below by the formation of a nocturnal temperature inversion. This decoupling reduces the frictional drag on air parcels at the top of the boundary layer, resulting in an acceleration of the wind (Blackadar, 1957; Thorpe and Guymer, 1977). Baroclinic (Holton, 2004) LLJs, such as coastal and ice-edge LLJs, are formed due to horizontal temperature differences that arise from differential heating and cooling of adjacent surfaces. This creates shallow frontal zones, and hence vertical wind shear, at the boundary between land–sea and ocean–ice (Beardsley et al., 1987; Chechin & Lüpkes, 2019; Dieudonné et al., 2023; McNider & Pielke, 1981). Similarly, valley LLJs are created by differential heating of sun-facing sloped terrain and shaded valleys in mountainous regions (Holton, 1967). All of these LLJs are associated with enhanced vertical and horizontal wind shear generating turbulent mixing.

Lagrangian dispersion models are used to forecast the concentration field of various pollutants in the atmosphere. In Lagrangian dispersion models, dispersion is modelled by tracing the motion of a large number of virtual particles that are tagged at the source to represent dust, aerosols, or gases; for example, carbon dioxide, nitrogen, or ozone. The mean particle positions are determined by the mean atmospheric flow, which is typically provided by output from a numerical weather prediction (NWP) model or by meteorological observations. The turbulent dispersion is treated statistically; that is, the standard deviation of

particle positions about their mean locations depends on the statistical characteristics of the turbulent flow. Within the boundary layer, semi-empirical parametrizations of these statistical characteristics have been developed by fitting theory to observations, resulting in expressions for the variance of a particle position as a function of travel time known as velocity variances $\sigma^2_{u,v,w}$. These velocity variances depend on the meteorological conditions and are related to the turbulent diffusion $K_{x,y,z}$ of pollutants over a typical time-scale of the eddy causing the diffusion: Lagrangian integral time-scale $\tau_{x,y,z}$. (For horizontal x, y and u, v, and for vertical z and w components respectively.) In the free troposphere, however, Lagrangian dispersion models typically assume that the velocity variances are "independent" of the meteorological conditions and are thus constant in space and time (referred to hereafter as a steady-state free troposphere, SS). Several case studies, using observed distributions of tracers, have attempted to estimate the magnitude of free-tropospheric diffusion (Legras et al., 2005; Schumann, 1996; Sillman et al., 1990) and have found that a large range of $K_{x,y,z}$ can result in agreement with observed profiles for different cases, largely because they consider very distinct meteorological situations (Hall & Waugh 1997). Thus, the observations are inconsistent with the use of spatially and temporally homogeneous $K_{x,y,z}$, and therefore the free troposphere is not in a steady state.

For aviation forecasting, space- and time-varying CAT parametrizations have been developed by combining theory and observations. As discussed by Hoskins and Bretherton (1972), horizontal deformation, horizontal shear, vertical deformation, and vertical shear may all form sharp gradients from initially weak gradients in both dynamically active and passive tracers. Thus, most CAT parametrizations include terms that represent these atmospheric processes derived from NWP temperature and wind fields (Sharman et al., 2006). For example, Ellrod and Knapp (1992) developed a parametrization based on the product of horizontal deformation and vertical wind shear. Similarly, Brown (1973) combines horizontal deformation, absolute vorticity, and vertical wind shear to estimate the eddy dissipation rate ϵ.

In this article, we focus on the lower part of the free troposphere as we aim to quantify the impact of a newly implemented space- and time-varying free-tropospheric turbulence parametrization scheme (hereafter VT) on the dispersion of pollutants emitted at the surface. Section 2 presents the dispersion modelling system, VT parametrization and tracer experiments. Section 3 presents an analysis of our case studies for enhanced offshore and onshore turbulence and a discussion of results. Section 4 quantifies the impact of the VT parametrization on the dispersion of a tracer released at the surface.

2 | METHOD

As noted in Section 1, CAT frequently occurs near the edges of jets where horizontal and vertical wind shears are large. Our study aims to evaluate the effect of a new VT parametrization on the dispersion of pollution. We focus on atmospheric conditions in which the effects of transient synoptic-scale features, such as fronts, are weak to highlight the potential impact of mesoscale LLJs. Thus, we have chosen two case study months during which the atmospheric conditions are largely quiescent, as we assume that such stable conditions will bring to the foreground the effects of the new VT parametrization.

In our case studies, we use NAME-III (v8.0) (hereafter NAME), which is a Lagrangian dispersion model and the Met Office NWP Unified Model (UM) in its global configuration (Walters et al., 2019). In Section 2.1 we detail the NWP data used, in Section 2.2 we provide details of the SS and VT turbulence parametrization, and in Section 2.3 we describe the tracer emissions. In Sections 2.4 and 2.5 we briefly describe the synoptic situation for each of the case study months. In Section 2.6 we provide details of the atmospheric monitoring used to validate our results.

We perform two experiments, the first using the existing fixed-value scheme, SS, and the second using the new spatial- and temporal-varying scheme, VT. We use the differences between these two experiments to quantify the impact of the VT parametrization on the atmospheric dispersion of surface-emitted pollutants. We run the experiments for the two case periods of July 2018 and April 2021.

The concentration fields from NAME are output on a gridded domain for Great Britain and the island of Ireland (hereafter Ireland) (Figure 1). The domain of the grid is from longitude −11.0° to +2.5° and latitude 49.0° to 60.0° N; the grid spacing is 0.23° longitude and 0.16° latitude (approximately 17 km), giving 58 points in longitude and 73 points in latitude; the vertical grid spacing is 50 m, with the lowest level at 25 m and highest level is at 2,975 m. The concentration fields are output hourly and represent the average over the hour. The boundary-layer depth (BLD) has a minimum of 40 m and a maximum of 4,000 m. The NAME simulations were performed on JASMIN (https://jasmin.ac.uk), the UK's collaborative data analysis and computing environment (Lawrence et al., 2013).

We partition the atmosphere near the surface into two regions, (i) the boundary layer and (ii) the free troposphere (Stull, 1999, chap. 1), using the BLD output from the Global UM. The method used to diagnose BLD is described in Lock et al. (2000); Lock (2001); and Brown et al. (2008), in essence, uses one of two methods: (a) for unstable conditions, it is the height at which an air

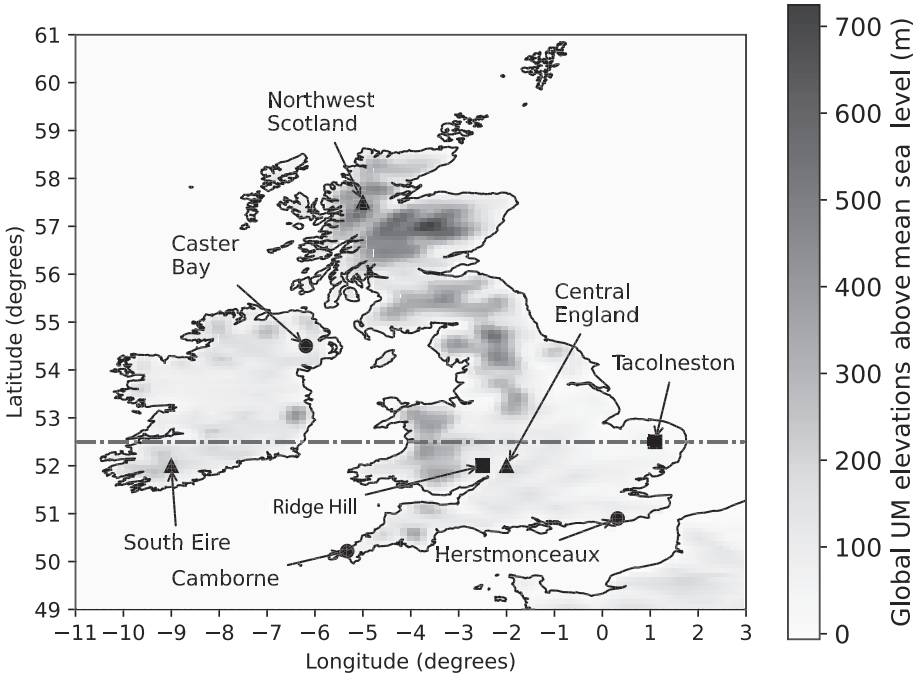

FIGURE 1 Global Unified Model land surface elevation map for Great Britain and Ireland. The simulations use virtual particles emitted at a constant rate over the land surface to represent the Radon-222. (No emissions over France.) The horizontal line is the location of vertical cross-sections. Locations: radiosonde stations (circles); UK Deriving Emissions linked to Climate Change greenhouse gas monitoring sites (squares); numerical weather prediction sampled points (triangles). [Colour figure can be viewed at wileyonlinelibrary.com]

parcel rising from the surface reaches neutral buoyancy; and (b) for stable conditions, it is when the Richardson index R_i is less than a critical value, set to 1 in the Global UM. This occurs when the turbulence produced by vertical wind shear overcomes the turbulent suppression due to the effects of stability.

2.1 | NWP data

The global NWP model incorporates observations using a hybrid four-dimensional data assimilation system (Clayton et al., 2013). Global NWP forecasts are initialized every 6 hr. A subset of the global model's fields is generated for use with NAME at a temporal resolution of 3 hr consisting of alternating model analyses and 3-hr forecasts. The meteorological fields have a horizontal grid length of 10 km at the Equator and 70 levels from the surface to 80 km, of which only the first 59 levels (surface to 30 km) are used for NAME applications. These meteorological fields are linearly interpolated in time and space within the NAME executable.

2.2 | Free-tropospheric turbulence parametrization scheme

One mechanism regulating the variability in subgrid-scale diffusion is Kelvin–Helmholtz instability, an instability occurring when significant shear exists between two layers of a fluid. If the shear is sufficiently large, it can distort the boundary into an amplifying wave that eventually breaks down into turbulence. In this section, we give a short summary of the theoretical basis and main assumptions used in the parametrization of CAT developed by Brown (1973). We then outline how we implement this parametrization in NAME.

2.2.1 | Brown's (1973) turbulence parametrization

The CAT parametrization developed by Brown (1973) is determined empirically but is based on a theory relating three mechanisms to turbulence generation: wind speed difference across a vertical layer, horizontal deformation, and absolute vorticity. The wind speed difference across a vertical layer represents vertical wind shear generation of turbulence. Horizontal deformation is included since it increases the horizontal temperature gradient, which, by thermal wind balance, also leads to enhanced vertical shear. The absolute vorticity term is included since positive vorticity advection, when the wind is perpendicular to the vorticity axis, enhances large-scale ascent in the atmosphere leading to atmospheric mixing that can generate CAT. This parametrization does not account for the generation of turbulence due to inertial instability. Inertial instability depends on the Earth's rotation and horizontal shear and/or curvature of the horizontal wind. It can generate turbulence wherever anticyclonic relative vorticity becomes larger than the Coriolis parameter. Thus, it occurs primarily in the Tropics, where the Coriolis parameter is small, but it can also generate turbulence in the extratropics near intense anticyclones.

2.2.2 | Parametrization of free tropospheric turbulence in NAME

NAME parametrizes free-tropospheric turbulence as a diffusion process represented by a turbulent diffusion parameter $K_{x,y,z}$ (Stull, 2000), where,

$$K_{x,y,z} = \left(\sigma_u^2\tau_u, \sigma_u^2\tau_u, \sigma_w^2\tau_w\right). \quad (1)$$

In the SS scheme, NAME uses fixed values for $\sigma_{u,w}^2$ and $\tau_{u,w}$; the current default values for $\sigma_{u,w}^2$ are 0.25 and 0.01 $m^2 \cdot s^{-2}$ for u and w respectively, and fixed values for $\tau_{u,w}$ are 300 s and 100 s for u and w respectively (Jones, 2017). We test a new parametrization scheme that parametrizes the spatial and temporal-varying free-tropospheric turbulence (VT). We do this by allowing $\sigma_{u,w}^2$ to vary depending on the eddy dissipation rate ϵ ($m^2 \cdot s^{-3}$), such that

$$\sigma_w^2 = \epsilon\tau_w, \quad (2)$$

Thus, in our new varying turbulence scheme both the vertical and horizontal diffusivities are modified. However, we note that turbulence does not play such a critical role in horizontal dispersion, as larger mesoscale motions typically dominate, so we focus on the implementation of the vertical component. We express ϵ using Brown's (1973) scheme,

$$\epsilon = \frac{(\Delta V)^2}{24}\Phi, \quad (3)$$

where ΔV is the change in the horizontal wind speed in the vertical, normalized across a depth of 500 m, and Φ represents the atmospheric horizontal deformation and absolute vorticity:

$$\Phi = \left(0.3\zeta_a^2 + D_{\text{shear}}^2 + D_{\text{stretch}}^2\right)^{1/2}, \quad (4)$$

where

$$\zeta_a = \left(\frac{\delta v}{\delta x} - \frac{\delta u}{\delta y} + f\right) \quad (5)$$

is the vertical component of the absolute vorticity,

$$D_{\text{shear}} = \left(\frac{\delta u}{\delta y} + \frac{\delta v}{\delta x}\right) \quad (6)$$

is the horizontal shearing deformation, and

$$D_{\text{stretch}} = \left(\frac{\delta u}{\delta x} - \frac{\delta v}{\delta y}\right) \quad (7)$$

is the horizontal stretching deformation, where f is the Coriolis parameter, u is the zonal (x) wind speed, and v is the meridional (y) wind speed. Note that we normalize ΔV to a depth of 500 m, since it has been found that 95% of turbulent patches are less than 500 m thick (Anderson, 1957). The parametrization has been implemented using finite differences between adjacent grid points.

2.3 | Tracer emissions description

We use an atmospheric tracer method to evaluate the impact of using VT on the dispersion of virtual particles. The atmospheric tracer we use is ^{222}Rn as it is a naturally occurring chemically inert radioactive gas with a half-life of 3.8 days (PubChem, 2023). As ^{222}Rn gas is chemically inert it is a useful tracer for studying atmospheric dynamics; for example, boundary-layer evolution (Galmarini, 2006; Vinuesa & Galmarini, 2007) and for estimation of local and regional greenhouse gas emissions (Grossi et al., 2016, 2018; Van Der Laan et al., 2010). A semi-idealized model is used to represent the uniform emission of ^{222}Rn from soil and rocks. The model emits ^{222}Rn at a constant rate of 1 g·hr^{-1} over the land surface represented at each land grid point of the Global UM land surface elevation map (Figure 1). The uniform emission uses virtual particles, with a maximum of 2×10^6 particles circulating within the domain; particles older than 48 hr are removed; these constraints are for computational efficiency and have no adverse effects on our results. The dispersion of ^{222}Rn is represented as an hourly air concentration on the output domain defined in Section 2.

2.4 | Summary of the synoptic conditions for July 2018

During July 2018, the synoptic conditions were dominated by high-pressure regions over Scandinavia and northern Europe, which were the main influences for weather conditions over the East Coast of England. These were broken with a few periods of unsettled weather, mostly towards the end of the month. The mean daytime UK temperature for this month was 17°C, which is 2°C above the 1981–2010 climate average. Most of the month was dry, with rainfall that was 70% of the climate average of 80 mm. The East Coast region was particularly dry for the month (Met Office, 2018; Prichard, 2018). This month was also notable for the sharp contrast in the NWP BLDs over the marine and land environments, with monthly means of 100 m and 2,000 m respectively. The low BLDs over the marine environment may be due to low sea-surface temperatures. The largely clear-sky conditions during this month result in strong surface heating during the daytime over the land when compared with the marine environment (due to the relative difference in their heat capacities), giving rise to a temperature gradient between land and sea.

2.5 | Summary of the synoptic conditions for April 2021

The month of April 2021 was dominated by anticyclonic conditions; high pressure was situated to the west of Great Britain at the start of the month and migrated eastwards towards the middle of the month. There was a short period when low-pressure systems brought unsettled conditions, but these were transient features, being replaced by a further high-pressure region migrating from west to east. The anticyclonic conditions were also dominated by clear sky during the day and night times, resulting in a strong diurnal temperature cycle, with night-time temperature minima being up to 3.0°C below the 1981–2010 climate average of 3.7°C, whereas daytime temperatures were close to the climate average of 10.9°C (Met Office, 2021; Prichard, 2021).

2.6 | Monitoring sites

Figure 1 shows the observation monitoring sites and NWP point locations used for assessing the effect of the VT scheme. The monitoring sites used are (a) radiosonde stations at Castor Bay, Camborne, and Herstmonceaux, used to obtain vertical profiles of wind and temperature; (b) tall tower sites, at Ridge Hill and Tacolneston, used to measure air concentrations of greenhouse gases and which are part of the UK's network for Deriving Emissions linked to Climate Change (DECC) (O'Doherty et al., 2020; Stanley et al., 2018; Stavert et al., 2019); and (c) sample points for NWP vertical profiles of wind and temperature. These latter points are chosen to assess the generality of our analysis within the NWP model domain and act as an independent sense at locations where there are likely to be no observations assimilated by the NWP model.

3 | RESULTS

We focus our analysis on the region of the free troposphere just above the BLD. We calculate monthly diurnal averages so that we can identify any systematic effect the new parametrization has on the dispersion of the radon tracer. We compute the monthly diurnal average for (a) the difference in the vertical velocity variance, which we define as $\Delta\sigma_w^2 = \sigma_w^2[\mathrm{VT}] - \sigma_w^2[\mathrm{SS}]$, and (b) the relative magnitude (RM%) of the monthly diurnal mean difference in the air concentration of ^{222}Rn (C) just above the BLD as

$$\mathrm{RM}\% = \frac{C[\mathrm{VT}] - C[\mathrm{SS}]}{C[\mathrm{VT}] + C[\mathrm{SS}]} \times 100,$$

where VT indicates the space–time-varying scheme and SS the steady-state scheme. The free troposphere is identified as being the first grid box in the output grid that is immediately above the grid box in which the NWP BLD is found. The free tropospheric turbulence parametrization in NAME is only applied at heights above the NWP BLD.

3.1 | Case study period July 2018

Figure 2 shows the monthly diurnal mean vertical velocity variance difference just above the BLD for July 2018. This shows that $\Delta\sigma_w^2$ has a diurnal pattern. At 0600 UTC, the magnitude of $\Delta\sigma_w^2$ has values between −0.01 and +0.04 $\mathrm{m}^2\cdot\mathrm{s}^{-2}$. By 1200 UTC, $\Delta\sigma_w^2$ over land has decreased. VT is smaller than the SS, as indicated by negative value (−0.01 $\mathrm{m}^2\cdot\mathrm{s}^{-2}$), whereas around the coastal regions there is an increase in VT as $\Delta\sigma_w^2$ is mostly positive (0.02–0.06 $\mathrm{m}^2\cdot\mathrm{s}^{-2}$), an increase of 200–600% on the SS default value. By early evening, 1800 UTC, the magnitude of $\Delta\sigma_w^2$ around the coast has increased to between 0.02 and 0.10 $\mathrm{m}^2\cdot\mathrm{s}^{-2}$. By 0000 UTC, this enhancement of turbulence around the coast decays (0.02–0.06 $\mathrm{m}^2\cdot\mathrm{s}^{-2}$), and by early morning, 0600 UTC, it has returned to a more quiescent state. Overall, these results show that $\Delta\sigma_w^2$ remains positive around the coast; that is, the vertical velocity variance is greater in the simulation with the VT scheme by up to two orders of magnitude.

We show in Figure 3 the effects of using the VT parametrization on the ^{222}Rn concentration. We interpret the results as follows. When RM% < 0, the air concentration $C[\mathrm{VT}] < C[\mathrm{SS}]$; that is, the ^{222}Rn concentration is higher using the SS scheme than when using the VT scheme for the same location and period. The opposite case applies when RM% > 0. These instances are depicted in Figure 3 as the dark and light regions respectively and follow the diurnal pattern of the $\Delta\sigma_w^2$ shown in Figure 2, where regions of enhanced σ_w^2 lead to a reduced mean air concentration of ^{222}Rn. (A similar diurnal pattern, not shown, is also evident for August 2018.) The ^{222}Rn concentrations are reduced over coastal regions by up to 40%, peaking at 1800 UTC.

We consider next the synoptic conditions that may give rise to this diurnal pattern. The general synoptic conditions for the UK are described in Section 2.4. In Figures 4 and 5 we examine the vertical cross-sections of the NWP climate at a sample latitude of 52.5° N, and where longitude points <10° W, 7° W to 4° W, and >1° E correspond to the North Atlantic Ocean, the Irish Sea, and the North Sea respectively (see also Figure 1). Figure 4 shows a vertical (z) cross-section of the monthly mean potential temperature (θ) at the hours corresponding

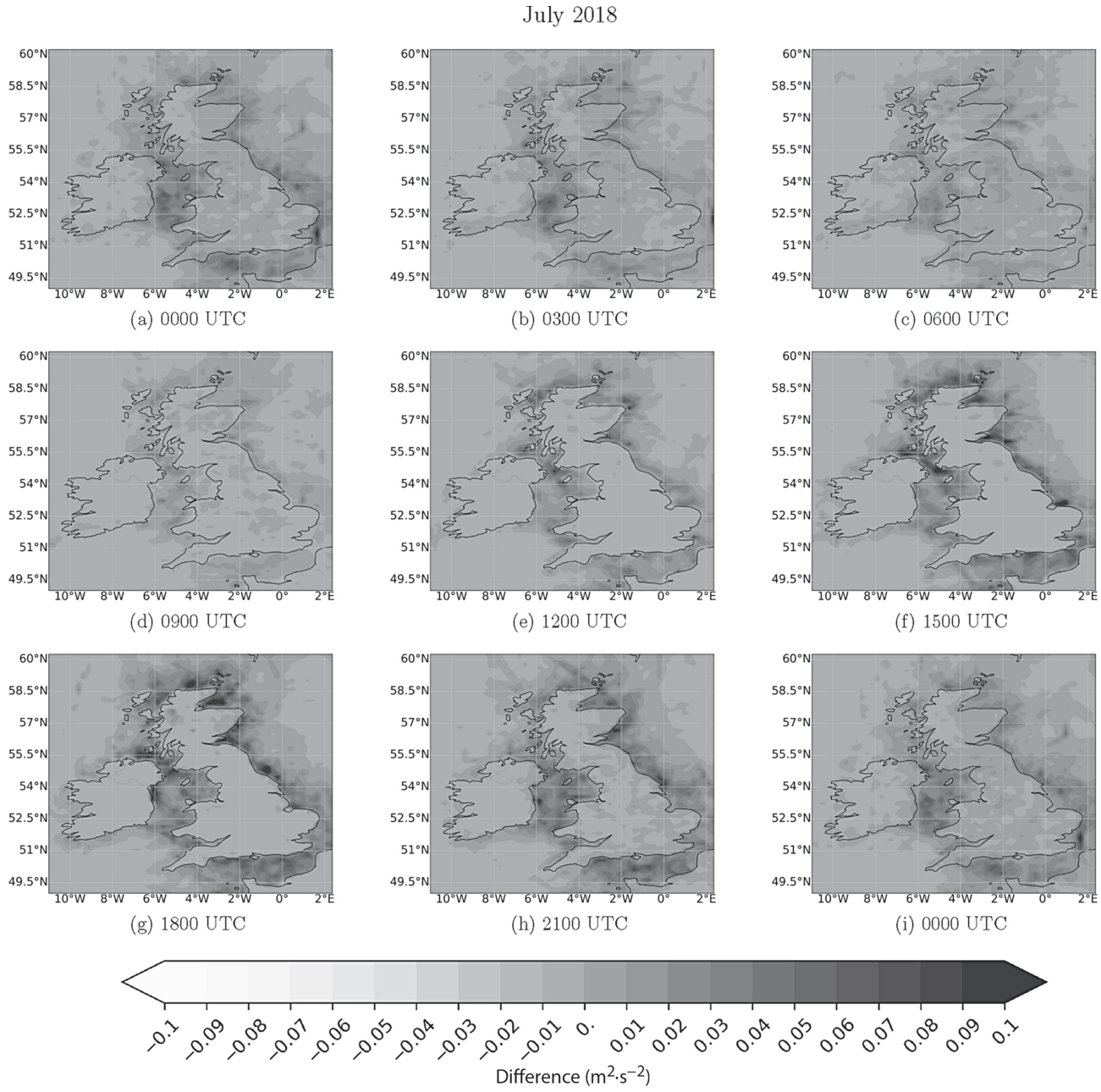

FIGURE 2 Diurnal evolution of the monthly mean difference of the vertical velocity variance (space–time varying minus steady state) just above the boundary-layer depth at three-hourly intervals for July 2018. [Colour figure can be viewed at wileyonlinelibrary.com]

to the NWP fields. These show that the free troposphere is stable ($d\theta/dz > 0$) and suppresses vertical mixing. However, between 1200 UTC and 1800 UTC and from the surface to 1,500 m there is a horizontal temperature gradient; thus, the atmosphere is baroclinic and there is vertical wind shear through thermal wind balance. The horizontal temperature gradient arises from the thermal contrast between the land and sea. The enhanced mixing peaks in the late afternoon, 1500 UTC, which is consistent with the maximum thermal contrast between land and sea. As the evening progresses, the BLD decreases, resulting in a decoupling of the air above the BLD from the effects of surface friction, causing it to accelerate. Figure 5 shows the corresponding cross-section for wind speed. Between the surface and 500 m, it is clear that LLJs form during the course of the day, and these are predominately at the coast.

We conclude from this case study that when the synoptic conditions are dominated by high pressure and weak synoptic-scale winds then we can expect to find enhancement of the vertical velocity variance due to the presence of coastal LLJs arising from baroclinic instability around

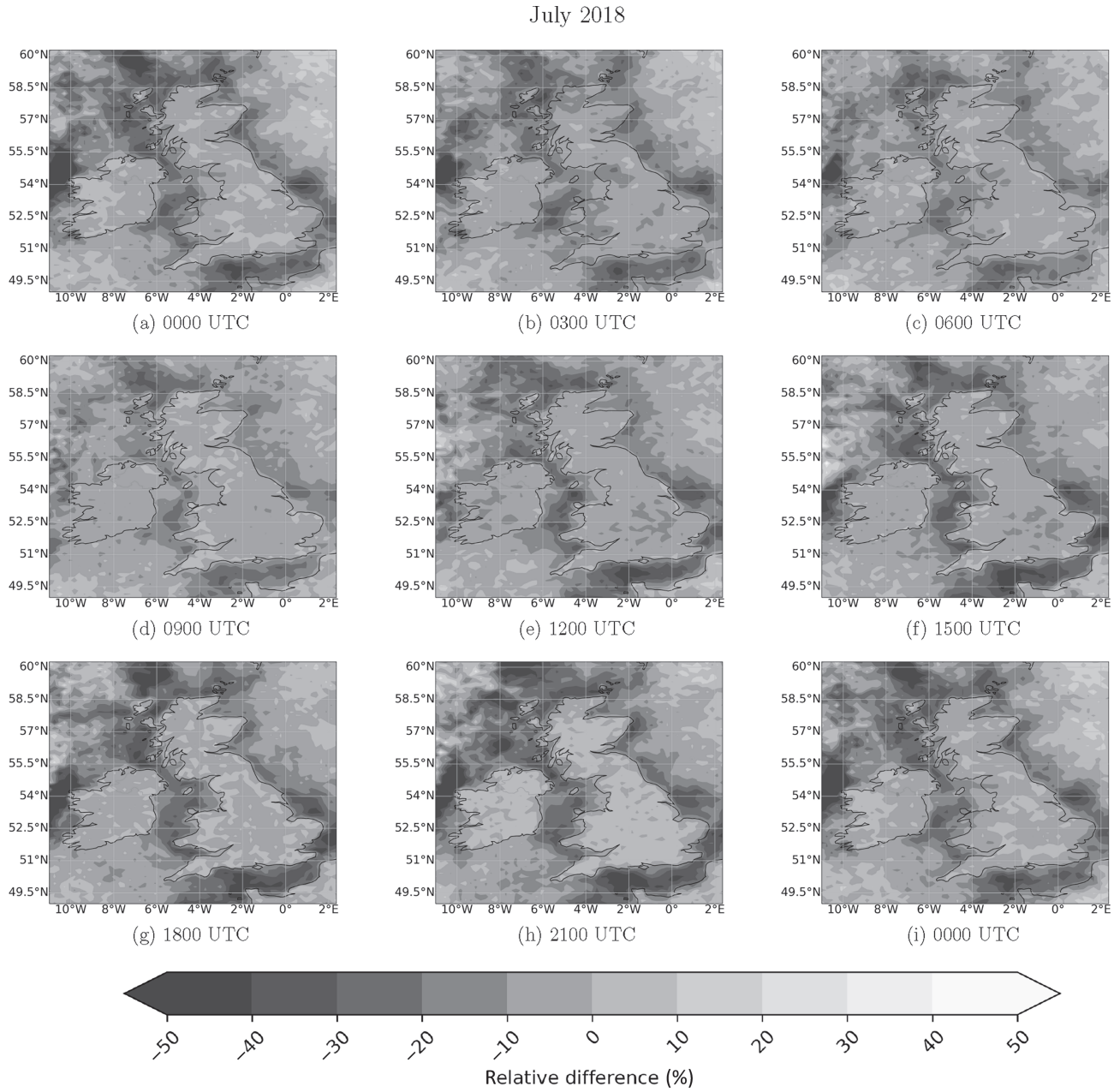

FIGURE 3 Diurnal evolution of the monthly mean relative difference of the radon-222 concentration (space–time varying minus steady state) just above the boundary-layer depth at three-hourly intervals for July 2018. [Colour figure can be viewed at wileyonlinelibrary.com]

the coast. The enhancement of vertical velocity variance is due to an increase in the vertical gradient of the horizontal wind speed.

3.2 | Case study for April 2021

In this section, we consider a similar high-pressure-dominated situation that arose in April 2021, as described in Section 2.5.

In Figure 6 we show $\Delta\sigma_w^2$ for April 2021. Here, we start our sequence at 1800 UTC, as we wish to emphasize the development of $\Delta\sigma_w^2$ that occurs overnight. We note that at 1800 UTC there is enhancement of the $\Delta\sigma_w^2$ around the coast. This enhancement is due to the presence of coastal LLJs, as discussed for case study 1, although their intensity is weaker by a factor of 2, which may be due to the weaker solar heating for this time of year. Around 0000 UTC there is an evolution of the $\Delta\sigma_w^2$ overland, especially in Scotland and northern, western, and southwestern regions of England. By 0600 UTC, there are indications that $\Delta\sigma_w^2$ is increasing in these regions, in addition to an increase in the geographic distribution of lower intensity $\Delta\sigma_w^2$ around the south and southeast. By 1200 UTC, the enhancement

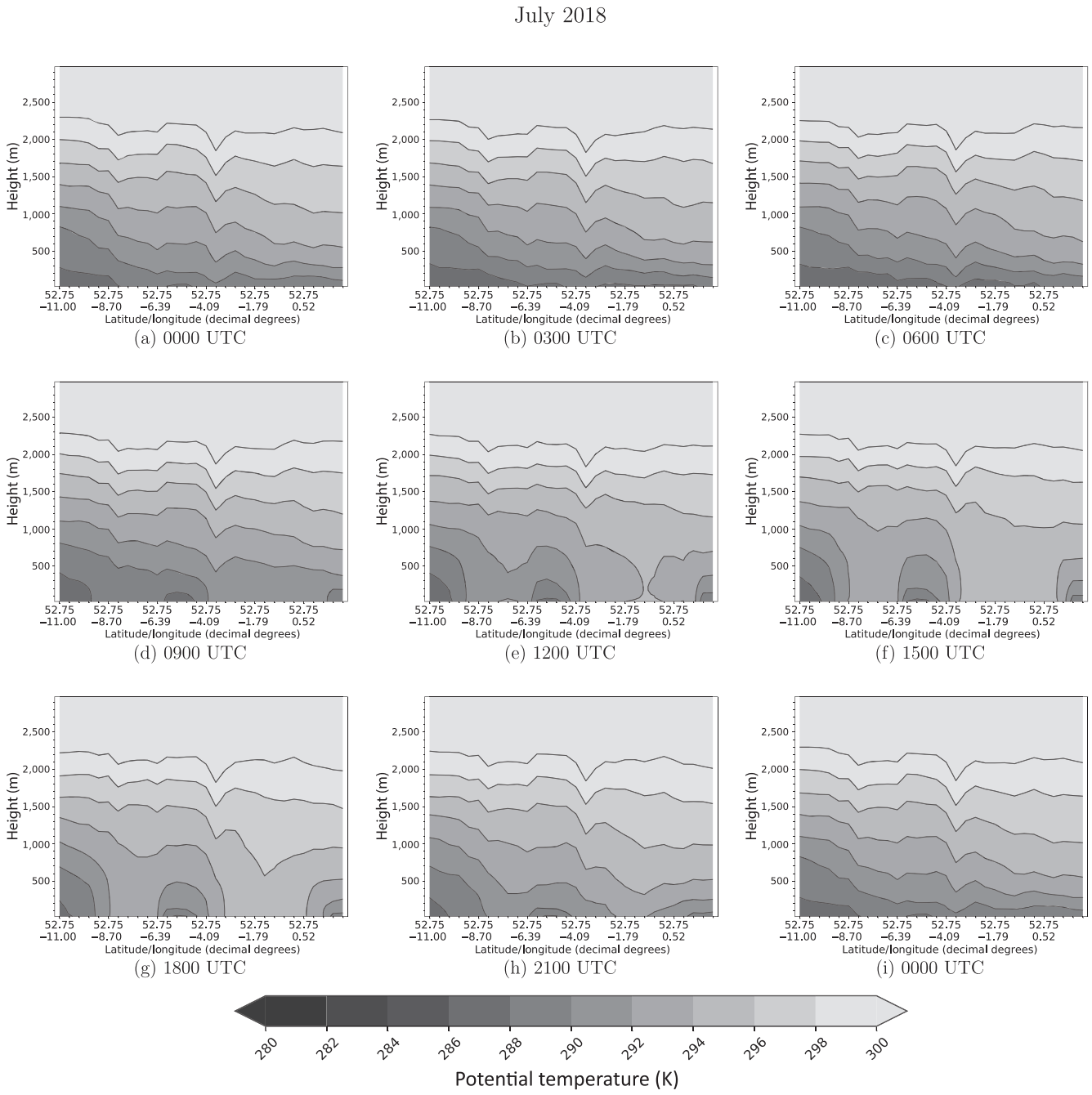

FIGURE 4 Diurnal evolution of the monthly mean of the vertical profile potential temperature (latitude 52.5° N) at three-hourly intervals for July 2018. Longitude points <10° W, 7° W to 4° W, and >1° E correspond to the North Atlantic Ocean, the Irish Sea, and the North Sea respectively. [Colour figure can be viewed at wileyonlinelibrary.com]

of the $\Delta\sigma_w^2$ over land has reduced. Figure 7 shows the corresponding effect on the air concentrations for ^{222}Rn, expressed as the relative magnitude. At 1800 UTC, we see that there is a higher concentration of ^{222}Rn around the coastal regions when using the SS scheme. In contrast, between 0000 UTC and 0600 UTC we note the greater ^{222}Rn concentration that evolves over land, which does not occur in case study 1. By 1200 UTC, the higher concentrations of ^{222}Rn over land have largely dissipated. We suggest that the cause of the enhancement of the vertical velocity variance over land is due to the nighttime synoptic conditions that give rise to nocturnal LLJs.

From late evening (>2100 UTC), radiative cooling over the land gives rise to the formation of temperature inversions. This has the effect of decoupling the air above the temperature inversion from the surface friction, leading to an acceleration of the wind. The peak of this effect is in the hours before sunrise. After sunrise, with

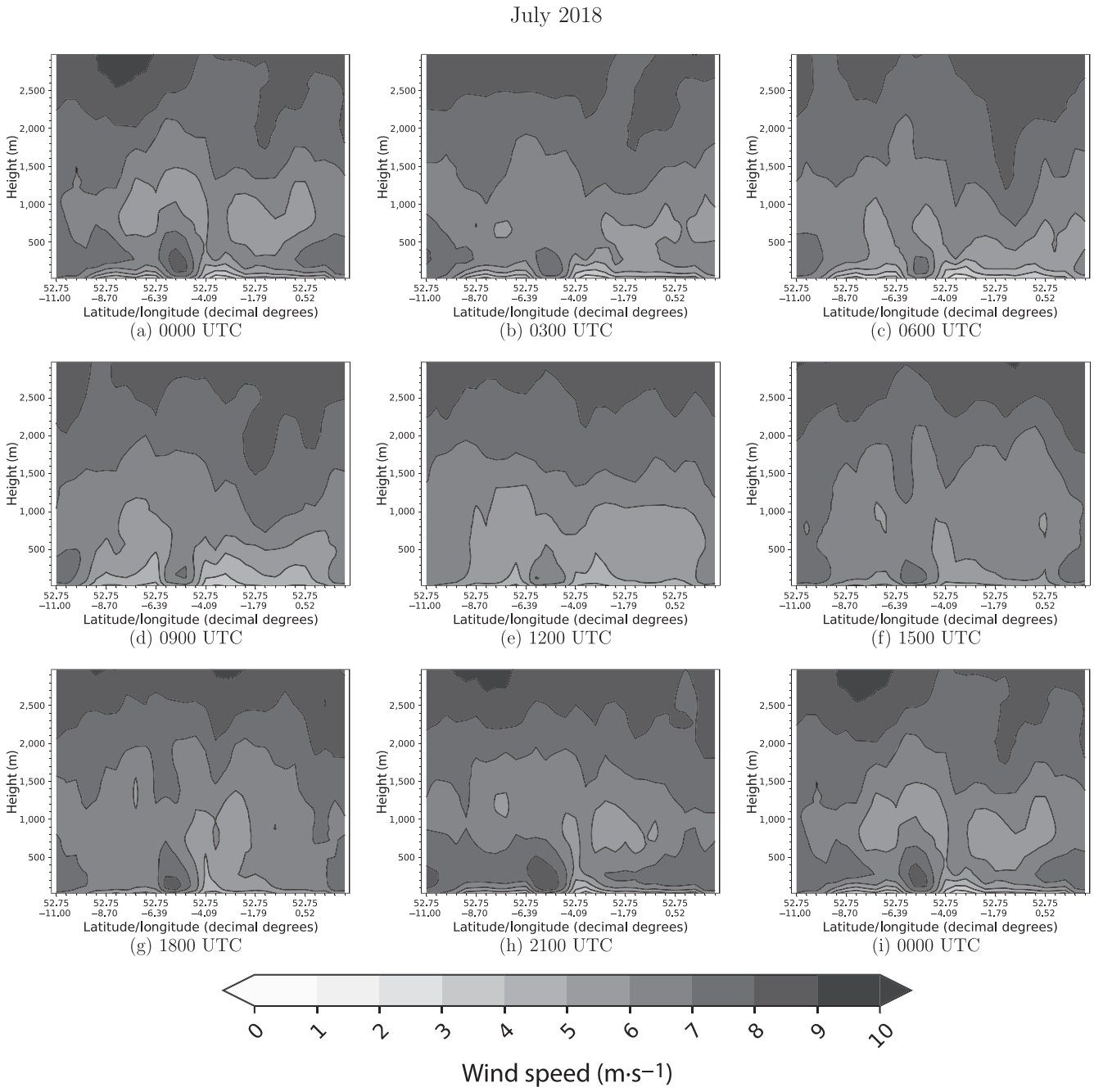

FIGURE 5 Diurnal evolution of the monthly mean of the vertical profile windspeed (latitude 52.5° N) at three-hourly intervals for July 2018. Longitude points are the same as in Figure 4. [Colour figure can be viewed at wileyonlinelibrary.com]

surface heating, the resulting increase in vertical mixing of warm air erodes the temperature inversion, dissipating the nocturnal LLJs.

Nocturnal LLJs typically form below 900 m and are characterized by wind speed maxima just above the location of a temperature inversion above the surface. Figure 8 shows the radiosonde vertical profiles for three meteorological observation stations: Castor Bay, Herstmonceaux, and Camborne, located in Northern Ireland, the south and southwest of England respectively. Each figure shows a maximum wind speed and a temperature inversion just above the BLD estimated from NWP. These profiles are characteristic of the presence of a nocturnal LLJ.

For case study 2, the synoptic conditions result in a strong temperature difference between the land and marine environment. However, unlike in case study 1, the land surface is much cooler, due to strong radiative cooling overnight, which gives rise to near-surface temperature inversions and low BLDs. The atmospheric flow just above the BLD becomes decoupled from the frictional effect of the surface. This leads to an increase in the horizontal wind speed just above the boundary layer,

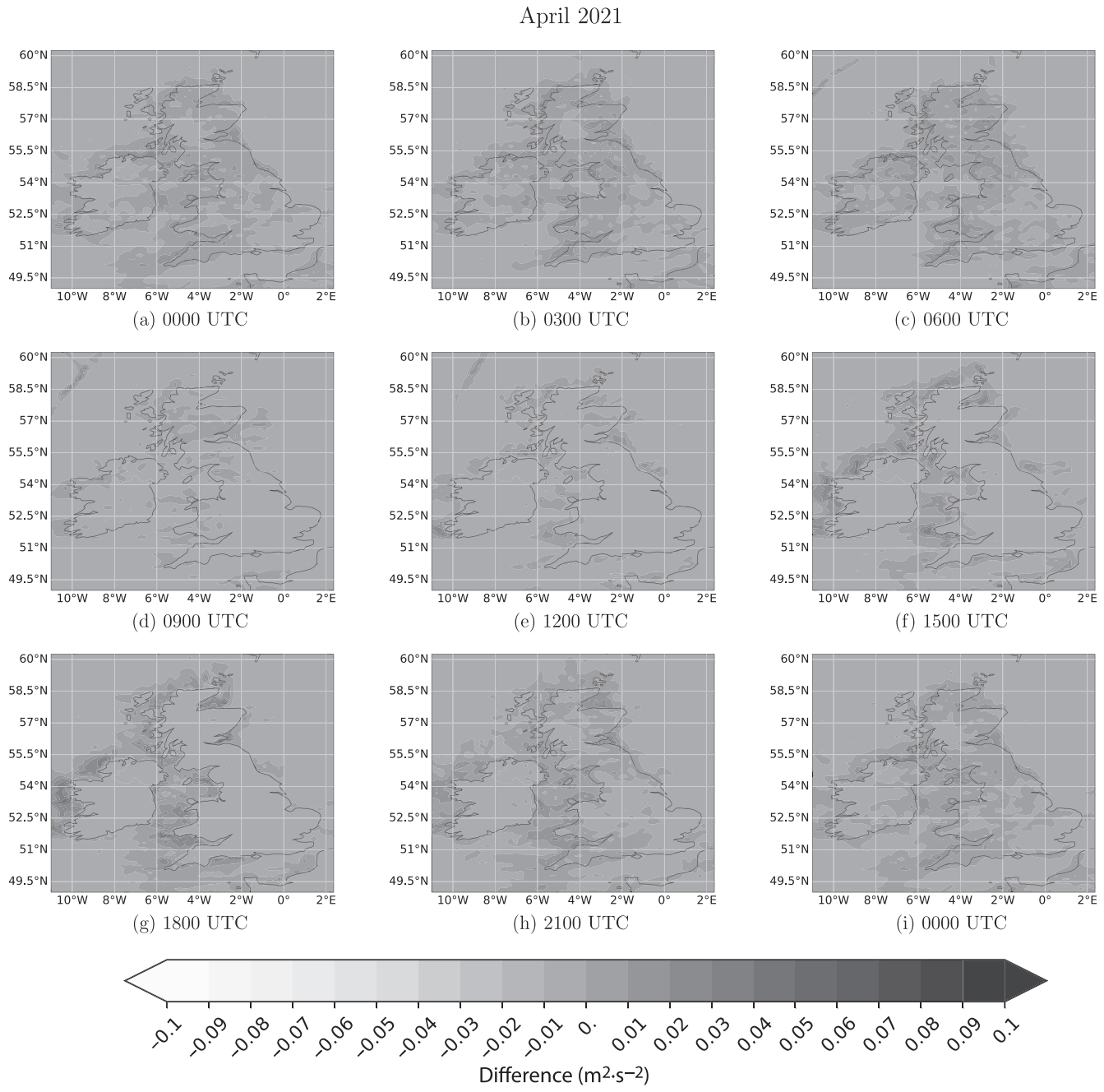

FIGURE 6 Diurnal monthly mean vertical velocity variance difference (space-time varying minus steady state) just above the boundary-layer depth at three-hourly intervals for April 2021. [Colour figure can be viewed at wileyonlinelibrary.com]

with a maximum speed below 1,000 m, which peaks in the early morning hours and decays rapidly shortly after sunrise. From these conditions, we infer the presence of nocturnal LLJs, which enhances the vertical velocity variance due to the increase in the vertical gradient of the horizontal wind speed. We conclude that, again, when the synoptic conditions are predominantly stable then we can expect to find enhancement of the vertical velocity variance due to the presence of nocturnal LLJs.

3.3 | Analysis of results

The lack of representation of space–time-varying turbulence in the free troposphere may lead to inaccurate estimations of local emissions in greenhouse gas inventory studies. Our case studies suggest that these inaccuracies may arise when the synoptic conditions are conducive to the formation of an LLJ just above the BLD that persists or reoccurs over an extended period; for example, several

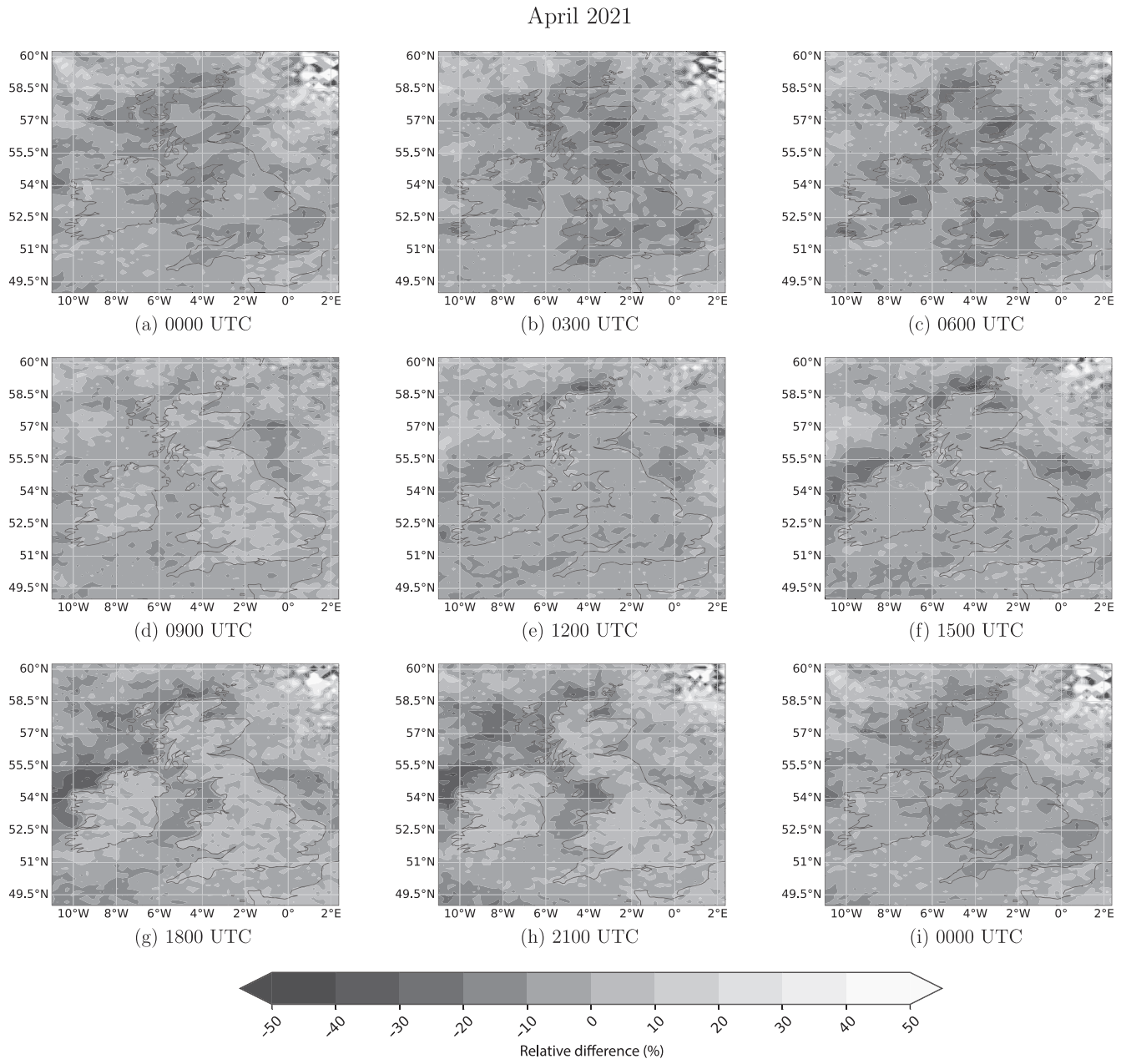

FIGURE 7 Diurnal monthly mean radon-222 concentration difference (space-time varying minus steady state) just above the boundary-layer depth at three-hourly intervals for April 2021. [Colour figure can be viewed at wileyonlinelibrary.com]

weeks. Figure 9 shows the monthly mean vertical profiles for NWP wind and temperatures at two DECC 2020 greenhouse gas monitoring sites and a radiosonde station. These profiles indicate that atmospheric conditions are conducive to the formation of nocturnal LLJs. (See Supporting Information Figure S1 for additional profiles.) It is during such periods that vertical velocity variance may be enhanced, leading to greater dispersion. This may be detected at tall tower monitoring stations (e.g., the DECC monitoring network), as the BLD falls below the inlet sensor height thus exposing it to free tropospheric turbulence (Arnold et al., 2022, personal communication). We note in Table 1 the number of occasions when the Met Office's NWP model BLD is estimated to fall below the inlet sensor height at the DECC monitoring sites; this occurs on average 15% of the time in the global NWP model.

We note, however, that the NWP BLD climatology may not perfectly represent the observed BLD climatology. Furthermore, the climatology of LLJs around the islands of Great Britain and Ireland is unknown. A recent study by Dieudonné et al. (2023), at Dunkerque, a coastal location to the English Channel, found LLJs occur on average around 5% of the time during year; occurring mostly during the late night (0000 to 0700 UTC) and the afternoon (1200

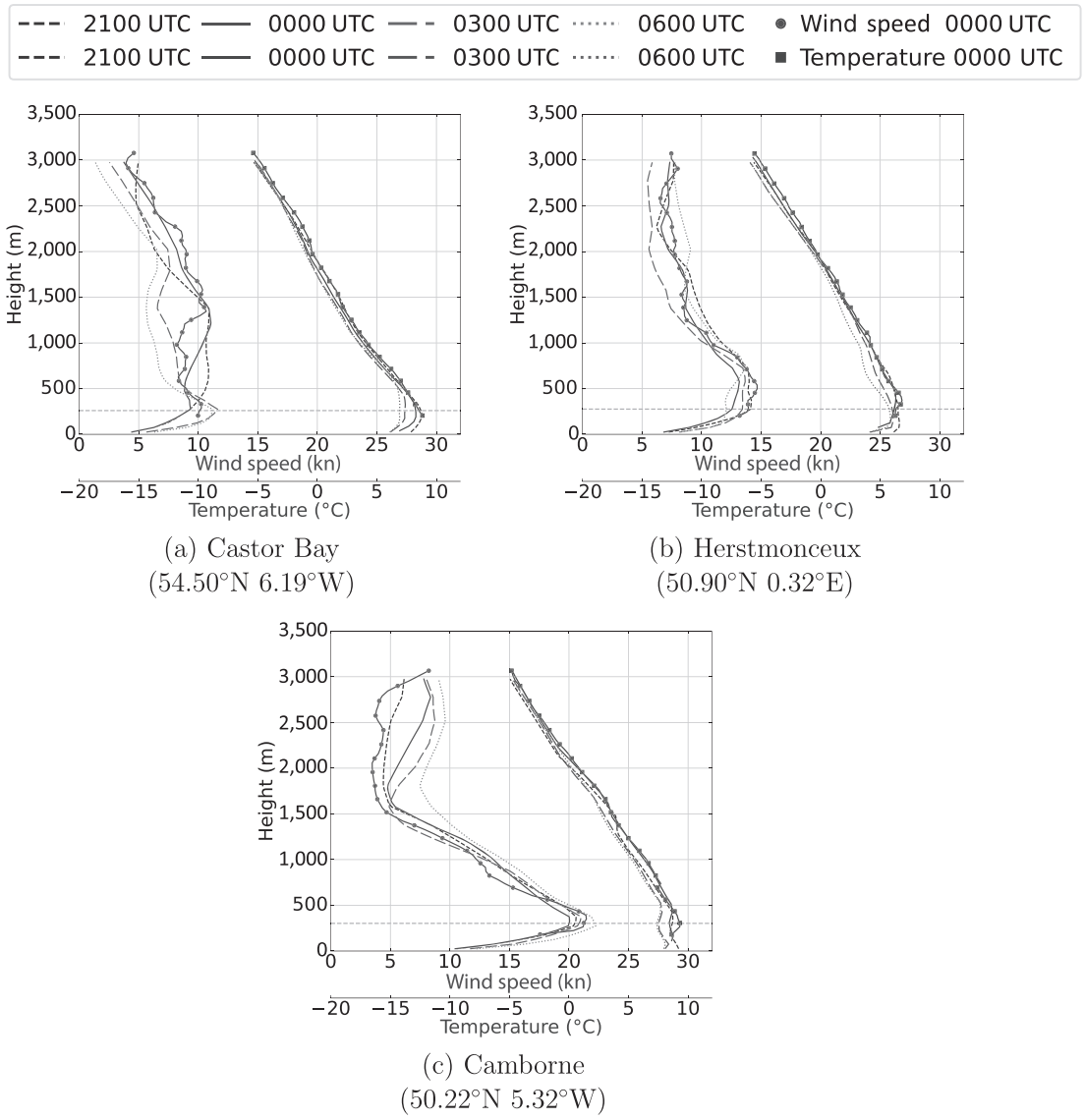

FIGURE 8 Weekly mean vertical profiles of wind speed (left) and temperature (right) for the period April 18–25, 2021, for radiosondes launched from (a) Castor Bay (03918), (b) Herstmonceux (03882), and (c) Camborne (03808). The solid lines with points are the radiosonde observations at 0000 UTC. The lines without points are for the corresponding vertical column of numerical weather prediction (NWP) data at the site. The NWP lines show the time evolution of the vertical profiles. The horizontal dashed line near the surface is the mean NWP boundary-layer depth. The numbers in parentheses are the corresponding World Meteorological Organization station identifiers/locations. Observation data are from the University of Wyoming Radiosonde Database. NWP data are from the Met Office Global Unified Model. [Colour figure can be viewed at wileyonlinelibrary.com]

to 1800 UTC); and during the spring and summer periods, when they are at their most intense, with a frequency two to three times greater than that of the autumn and winter periods. Our case studies appear to be consistent with these observations.

It is clear from our results that the inclusion of the free tropospheric VT parametrization has incorporated turbulent mixing that has hitherto not been represented within the dispersion model; that is, that associated with LLJs. In their review article, Wei et al. (2023) suggest that LLJs are a common feature and they discuss the implications this may have on the dispersion of gases and particulates. Wei et al. (2023) indicate that LLJs have at least two effects on air concentrations: (a) decreases due to long-range advection of pollutants above the LLJ (Banta et al., 1998; Corsmeier et al., 1997; Klein et al., 2019; Martins et al., 2018) and (b) increases below the LLJ due to downward momentum brought about by the enhanced vertical wind shear (Fiedler et al., 2013; Karipot et al., 2006; Kulkarni et al., 2016; Schepanski et al., 2009). Our results are consistent with the first of these effects. We find no evidence of a significant increase in concentrations

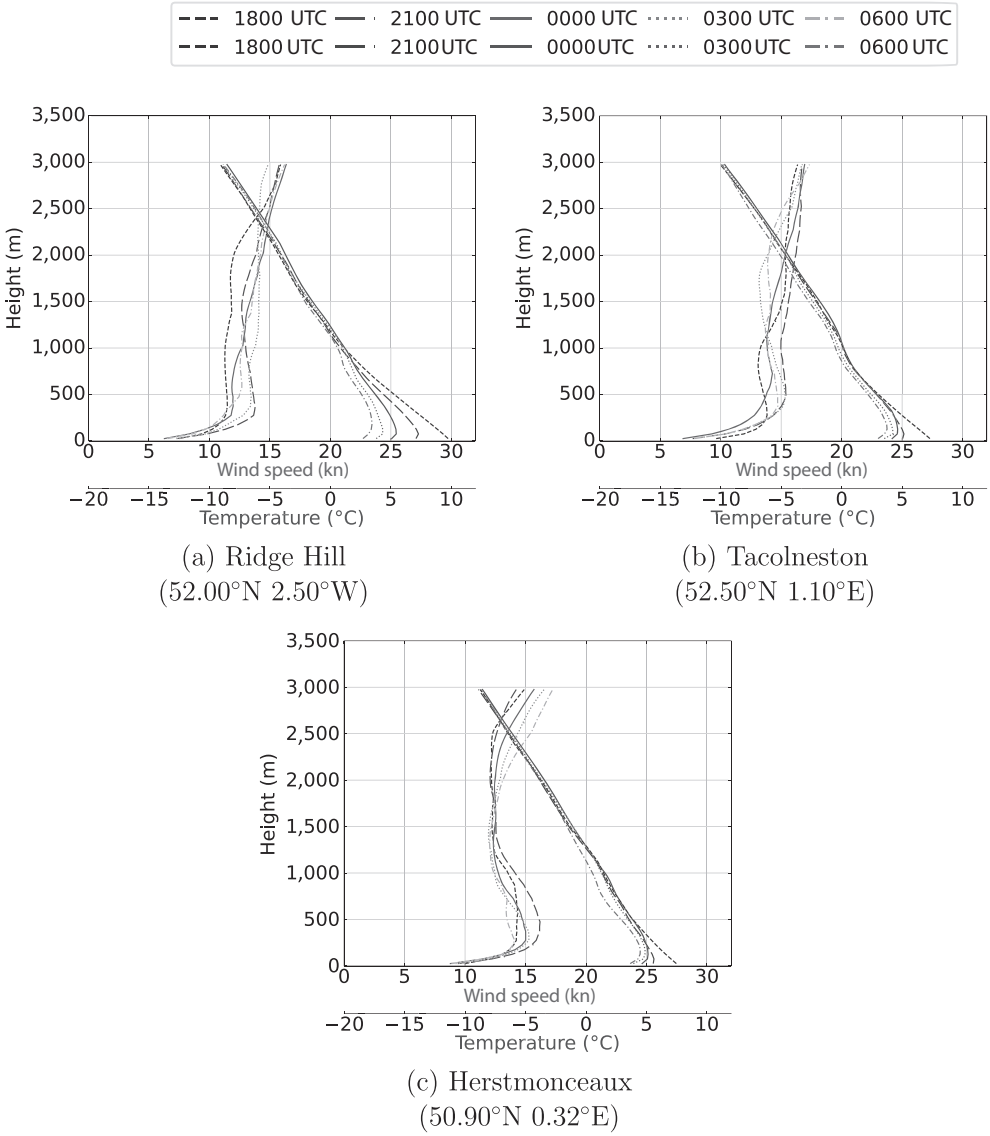

(a) Ridge Hill (52.00°N 2.50°W)

(b) Tacolneston (52.50°N 1.10°E)

(c) Herstmonceaux (50.90°N 0.32°E)

FIGURE 9 Monthly mean numerical weather prediction (NWP) vertical profiles of wind speed (left) and temperature (right) overnight for April 2021 at monitoring sites Ridge Hill and Tacolneston and for Herstmonceux radiosonde station. NWP data from the Met Office Global Unified Model. [Colour figure can be viewed at wileyonlinelibrary.com]

TABLE 1 Percentage of time the NWP BLD was below the inlet sensor height at the DECC greenhouse gas monitoring sites.

		Percentage Time NWP BLD < Sensor Height (%)		
		UKV	Global model	
Monitoring site	**Sensor height (m)**	**2015–2020**	**July 2018**	**April 2021**
Bilsdale	248	44	18	26
Tacolneston	175	33	21	21
Heathfield	100	25	16	12
Ridge Hill	75	20	10	17
Sample size (hr)		48,168	744	720

Note: Monitoring sites at Mace Head and Weybourne are excluded as their inlet sensor heights are less than 40 m, which is the minimum BLD set in the UK Met Office's Numerical Atmospheric-dispersion Modelling Environment.

Abbreviations: BLD, boundary-layer depth; DECC, UK's Deriving Emissions linked to Climate Change network; NWP, numerical weather prediction; UKV, Met Office limited-area model.

below the LLJ, but we note that this may be because we are considering a ground release of radon. Pollutants such as ozone, with a tropospheric reservoir, may well be mixed downwards towards the surface by the enhanced turbulence associated with LLJs (Corsmeier et al., 1997; Klein et al., 2019). Wei et al. (2023) conclude their review with the recommendation that current turbulence parametrizations should be improved to capture and represent the interaction between LLJs and the boundary layer and its effects on the dispersion of atmospheric gases and particulates.

4 | CONCLUSIONS

In this study, we have tested a new parametrization scheme to represent the spatial and temporal variability of atmospheric turbulence in the free troposphere within the Met Office's atmospheric dispersion model NAME. We have investigated the synoptic conditions in two case studies, July 2018 and April 2021, in which the free-tropospheric turbulence parametrization scheme gave rise to an enhancement of the vertical velocity variance, which has a diurnal cycle. The synoptic conditions are characterized by high-pressure regions (situated in and around the islands of Great Britain and Ireland) that persisted for several weeks, resulting in a strong diurnal temperature gradient between the land and marine environments and the subsequent formation of LLJs due either to baroclinic instability or inertial oscillations. The presence of the LLJs leads to an enhancement of the vertical velocity variance, and thus low-altitude atmospheric turbulence in the free troposphere. This had the effect of decreasing air concentrations of modelled ^{222}Rn in regions where this atmospheric turbulence occurs and increasing it elsewhere.

We conclude that without a space–time-varying free-tropospheric turbulence scheme the atmospheric dispersion may be significantly underestimated under synoptic conditions that are favourable for LLJ formation. Underestimation of dispersion can potentially result in inaccurate, systematic overestimation of local pollution concentrations, which, from our case studies, may be as much as 20% to 40% just above the BLD, whereas below the BLD our case studies suggest a variation of ±10%. Such inaccuracies may affect the results of studies that use dispersion modelling; for example, top-down greenhouse gas inventory studies or long-range transport of polluting gases and radionuclides. Furthermore, without a space–time-varying scheme, the background free-tropospheric turbulence may also be overestimated.

We note that different NWP models will use different schemes and criteria to estimate the boundary layer depth, for example, the Met Office limited area model, UKV, uses $R_i < 0.25$ whereas their global model uses $R_i < 1.0$. Therefore the activation of the new turbulence scheme will be dependent on the NWP model. Nonetheless, these NWP models are used to inform studies on the source attribution of greenhouse gases and are an additional source of uncertainty.

Therefore, we suggest further studies are required. For instance, using a wider domain should be investigated; for example, the European mainland. The results from our second case study suggest that similar atmospheric behaviour may be found over land, thus affecting dispersion over a wider domain. Also, the impact of the new turbulence scheme for inverse modelling using the latest version of NAME (v8.3+) should be evaluated, wherein the new parametrization can use the Met Office's limited-area model, UKV (Milan et al., 2020), which has one-hourly NWP fields and a horizontal grid spacing of 1.5 km.

Validation of our study is difficult to assess for at least two reasons: (a) the transient nature of the atmospheric phenomenon we seek to detect; and (b) the limited availability of near-surface observations for vertical profiles of wind and temperature over Great Britain and Ireland, and the surrounding marine environment. Therefore, further research in obtaining upper air observations from which the free-tropospheric vertical velocity variance could be obtained directly or derived would help with the verification of the modelled values.

AUTHOR CONTRIBUTIONS

Andrew K. Mirza: conceptualization; data curation; formal analysis; investigation; methodology; project administration; resources; software; validation; visualization; writing – original draft; writing – review and editing. **Helen F. Dacre:** conceptualization; formal analysis; funding acquisition; investigation; methodology; resources; supervision; validation; visualization; writing – original draft; writing – review and editing. **Chun Hay Brian Lo:** data curation; investigation; resources; software; visualization; writing – review and editing.

ACKNOWLEDGEMENTS

We would like to thank Alistair Manning for his review and comments on the draft version of the manuscript. We also thank Helen Webster and Emma Kendall at the Met Office for technical help with implementing the varying turbulence scheme in NAME. We also thank the two anonymous

reviewers for their time, commitment, and constructive comments to improve our manuscript.

FUNDING INFORMATION

Andrew K. Mirza and Helen F. Dacre were supported by the United Kingdom's Natural Environmental Sciences Research Council (NERC) project Detection and Attribution of Regional Greenhouse Gas Emissions in the UK (DARE-UK) grant number NE/S004505/1; Brian Lo was supported by a scholarship from the Department of Meteorology at the University of Reading and a Met Office CASE studentship.

DATA AVAILABILITY STATEMENT

The datasets used in this study: Modelled NAME data are available from the University of Reading's Research Data Archive; radiosonde data are available from the Department of Atmospheric Science, University of Wyoming (https://weather.uwyo.edu/upperair/sounding.html); and the Met Office Numerical Weather Prediction data, contact enquiries@metoffice.gov.uk. The availability and use of these data will be subject to their respective licensing conditions.

ORCID

Andrew K. Mirza https://orcid.org/0000-0001-6350-9080
Helen F. Dacre https://orcid.org/0000-0003-4328-9126
Chun Hay Brian Lo https://orcid.org/0000-0001-7661-7080

REFERENCES

Anderson, A.D. (1957) Free-air turbulence. *Journal of the Atmospheric Sciences*, 14(6), 477–494. https://doi.org/10.1175/1520-0469(1957)014<0477:FAT>2.0.CO;2

Arnold, T., Kikaj, D. & Wenger, A. (2022) Private communication.

Banta, R.M., Senff, C.J., White, A.B., Trainer, M., McNider, R.T., Valente, R.J. et al. (1998) Daytime buildup and nighttime transport of urban ozone in the boundary layer during a stagnation episode. *Journal of Geophysical Research: Atmospheres*, 103(D17), 22519–22544. https://agupubs.onlinelibrary.wiley.com/doi/abs/10.1029/98JD01020

Barad, M. (1958) *Project prairie grass, a field program in diffusion: volume 1*. Air Force Cambridge Research Center (U.S.). Bedford, MA: Geophysics Research Directorate. https://apps.dtic.mil/sti/tr/pdf/AD0152572.pdf

Barsotti, S., Neri, A. & Scire, J.S. (2008) The VOL-CALPUFF model for atmospheric ash dispersal: 1. Approach and physical formulation. *Journal of Geophysical Research: Solid Earth*, 113(B3), B03208. https://agupubs.onlinelibrary.wiley.com/doi/abs/10.1029/2006JB004623

Beardsley, R., Dorman, C., Friehe, C., Rosenfeld, L. & Winant, C. (1987) Local atmospheric forcing during the Coastal Ocean dynamics experiment: 1. A description of the marine boundary layer and atmospheric conditions over a northern California upwelling region. *Journal of Geophysical Research: Oceans*, 92(C2), 1467–1488. https://doi.org/10.1029/JC092iC02p01467

Blackadar, A.K. (1957) Boundary Layer wind maxima and their significance for the growth of nocturnal inversions. *Bulletin of the American Meteorological Society*, 38(5), 283–290. https://doi.org/10.1175/1520-0477-38.5.283

Bonadonna, C., Folch, A., Loughlin, S. & Puempel, H. (2012) Future developments in modelling and monitoring of volcanic ash clouds: outcomes from the first IAVCEI-WMO workshop on ash dispersal forecast and civil aviation. *Bulletin of Volcanology*, 74(1), 1–10. Available from: https://doi.org/10.1007/s00445-011-0508-6

Brown, A.R., Beare, R.J., Edwards, J.M., Lock, A.P., Keogh, S.J., Milton, S.F. et al. (2008) Upgrades to the Boundary-Layer Scheme in the Met Office Numerical Weather Prediction Model. *Boundary-Layer Meteorology*, 128(1), 117–132. https://doi.org/10.1007/s10546-008-9275-0

Brown, R. (1973) New indices to locate clear-air turbulence. *Meteorological Magazine*, 102, 347–361. https://digital.nmla.metoffice.gov.uk/

Chechin, D. & Lüpkes, C. (2019) Baroclinic low-level jets in Arctic marine cold-air outbreaks. In: *IOP Conference Series: Earth and Environmental Science*, Vol. 231. IOP Publishing, 012011. https://iopscience.iop.org/issue/1755-1315/231/1

Clayton, A.M., Lorenc, A.C. & Barker, D.M. (2013) Operational implementation of a hybrid ensemble/4-D Var global data assimilation system at the Met Office. *Quarterly Journal of the Royal Meteorological Society*, 139(675), 1445–1461. https://rmets.onlinelibrary.wiley.com/doi/abs/10.1002/qj.2054

Corsmeier, U., Kalthoff, N., Kolle, O., Kotzian, M. & Fiedler, F. (1997) Ozone concentration jump in the stable nocturnal boundary layer during a LLJ-event. *Atmospheric Environment*, 31(13), 1977–1989. https://www.sciencedirect.com/science/article/pii/S1352231096003585

D'Amours, R., Alain Malo, T.F.J.W.J.-P.G. & Servranckx, R. (2015) The Canadian Meteorological Centre's Atmospheric Transport and Dispersion Modelling Suite. *Atmosphere-Ocean*, 53(2), 176–199. Available from: https://doi.org/10.1080/07055900.2014.1000260

Dacre, H., Grant, A., Harvey, N., Thomson, D., Webster, H. & Marenco, F. (2015) Volcanic ash layer depth: processes and mechanisms. *Geophysical Research Letters*, 42(2), 637–645. https://doi.org/10.1002/2014GL062454

Dieudonné, E., Delbarre, H., Sokolov, A., Ebojie, F., Augustin, P. & Fourmentin, M. (2023) Characteristics of the low-level jets observed over Dunkerque (North Sea French coast) using 4 years of wind lidar data. *Quarterly Journal of the Royal Meteorological Society*, 149(754), 1745–1768. https://rmets.onlinelibrary.wiley.com/doi/abs/10.1002/qj.4480

Draxler, R.R. & Hess, G.D. (1998) An overview of the HYSPLIT_4 modeling system for trajectories, dispersion, and deposition. *Australian Meteorological Magazine*, 47, 295–308. https://www.researchgate.net/profile/GHess/publication/239061109_An_overview_of_the_HYSPLIT_4_modelling_system_for_trajectories/links/004635374253416d4e000000/An-overview-of-the-HYSPLIT-4-modelling-system-for-trajectories.pdf

Ellrod, G.P. & Knapp, D.I. (1992) An objective clear-air turbulence forecasting technique: verification and operational use.

Weather and Forecasting, 7(1), 150–165. https://doi.org/10.1175/1520-0434(1992)007<0150:AOCATF>2.0.CO;2

Ferrero, E., Alessandrini, S., Meech, S., Rozoff, C. & Oettl, D. (2023) Comparison of two turbulence parameterisations for the simulation of the concentration variance dispersion. *Air Quality, Atmosphere & Health*, 16(1), 49–60. Available from: https://doi.org/10.1007/s11869-022-01268-y

Fiedler, S., Schepanski, K., Heinold, B., Knippertz, P. & Tegen, I. (2013) Climatology of nocturnal low-level jets over north africa and implications for modeling mineral dust emission. *Journal of Geophysical Research: Atmospheres*, 118(12), 6100–6121. https://agupubs.onlinelibrary.wiley.com/doi/abs/10.1002/jgrd.50394

Galmarini, S. (2006) One year of ^{222}Rn concentration in the atmospheric surface layer. *Atmospheric Chemistry and Physics*, 6(10), 2865–2886. https://acp.copernicus.org/articles/6/2865/2006/

Gifford, F. (1959) *Statistical Properties of A Fluctuating Plume Dispersion Model*. Advances in Geophysics, Vol. 6. Elsevier, pp. 117–137. https://www.sciencedirect.com/science/article/pii/S0065268708600990

Grossi, C., Àgueda, A., Vogel, F.R., Vargas, A., Zimnoch, M., Wach, P. et al. (2016) Analysis of ground-based ^{222}Rn measurements over Spain: Filling the gap in southwestern Europe. *Journal of Geophysical Research: Atmospheres*, 121(18), 11021–11037. https://agupubs.onlinelibrary.wiley.com/doi/abs/10.1002/2016JD025196

Grossi, C., Vogel, F.R., Curcoll, R., Àgueda, A., Vargas, A., Rodó, X. et al. (2018) Study of the daily and seasonal atmospheric CH_4 mixing ratio variability in a rural Spanish region using ^{222}Rn tracer. *Atmospheric Chemistry and Physics*, 18(8), 5847–5860. https://acp.copernicus.org/articles/18/5847/2018/

Hall, T.M. & Waugh, D. (1997) Tracer transport in the tropical stratosphere due to vertical diffusion and horizontal mixing. *Geophysical Research Letters*, 24(11), 1383–1386.

Hanna, S.R. (1981) Lagrangian and Eulerian Time-Scale Relations in the Daytime Boundary Layer. *Journal of Applied Meteorology and Climatology*, 20(3), 242–249. https://doi.org/10.1175/1520-0450(1981)020<0242:LAETSR>2.0.CO;2

Harvey, N.J., Huntley, N., Dacre, H.F., Goldstein, M., Thomson, D. & Webster, H. (2018) Multi-level emulation of a volcanic ash transport and dispersion model to quantify sensitivity to uncertain parameters. *Natural Hazards and Earth System Sciences*, 18(1), 41–63. https://nhess.copernicus.org/articles/18/41/2018/

Holton, J.R. (1967) The diurnal boundary layer wind oscillation above sloping terrain. *Tellus*, 19(2), 200–205. https://doi.org/10.1111/j.2153-3490.1967.tb01473.x

Holton, J.R. (2004) *An Introduction to Dynamic Meteorology*, 4th edition. (Chapter 8). Burlington, MA: International Geophysics: Elsevier Science.

Hoskins, B.J. & Bretherton, F.P. (1972) Atmospheric frontogenesis models: mathematical formulation and solution. *Journal of the Atmospheric Sciences*, 29, 11–37. https://doi.org/10.1175/1520-0469(1972)029<0011:AFMMFA>2.0.CO;2

Jones, A. (2004) Atmospheric dispersion modelling at the Met Office. *Weather*, 59(11), 311–316. https://rmets.onlinelibrary.wiley.com/doi/abs/10.1256/wea.106.04

Jones, A. (2017) *NAME Technical Specification Document A01, User Guide for NAME (Section1.7.4.3)*, Technical Report. Met Office, Exeter, United Kingdom.

Jones, A., Thomson, D., Hort, M. & Devenish, B. (2007) The U.K. Met Office's Next-Generation Atmospheric Dispersion Model, NAME III (pp 580-589). In: Borrego, C., Norman, AL. (Eds.), *Air Pollution Modeling and Its Application XVII*. Boston, MA: Springer. https://doi.org/10.1007/978-0-387-68854-1_62

Karipot, A., Leclerc, M.Y., Zhang, G., Martin, T., Starr, G., Hollinger, D. et al. (2006) Nocturnal CO2 exchange over a tall forest canopy associated with intermittent low-level jet activity. *Theoretical and Applied Climatology*, 85(3), 243–248. Available from: https://doi.org/10.1007/s00704-005-0183-7

Klein, A., Ravetta, F., Thomas, J.L., Ancellet, G., Augustin, P., Wilson, R. et al. (2019) Influence of vertical mixing and nighttime transport on surface ozone variability in the morning in Paris and the surrounding region. *Atmospheric Environment*, 197, 92–102. https://www.sciencedirect.com/science/article/pii/S135223101830699X

Kulkarni, P.S., Dasari, H.P., Sharma, A., Bortoli, D., Salgado, R. & Silva, A. (2016) Nocturnal surface ozone enhancement over Portugal during winter: Influence of different atmospheric conditions. *Atmospheric Environment*, 147, 109–120. https://www.sciencedirect.com/science/article/pii/S1352231016307749

Lawrence, B.N., Bennett, V.L., Churchill, J., Juckes, M., Kershaw, P., Pascoe, S. et al. (2013) Storing and manipulating environmental big data with JASMIN, Paper presented at '2013 IEEE international conference on big data.' pp. 68–75. https://doi.org/10.1109/BigData.2013.6691556

Legras, B., Pisso, I., Berthet, G. & Lefèvre, F. (2005) Variability of the Lagrangian turbulent diffusion in the lower stratosphere. *Atmospheric Chemistry and Physics*, 5(6), 1605–1622. https://doi.org/10.5194/acp-5-1605-2005

Lock, A.P. (2001) The Numerical Representation of Entrainment in Parameterizations of Boundary Layer Turbulent Mixing. *Monthly Weather Review*, 129(5), 1148–1163. https://doi.org/10.1175/1520-0493(2001)129<1148:TNROEI>2.0.CO;2

Lock, A.P., Brown, A.R., Bush, M.R., Martin, G.M. & Smith, R.N.B. (2000) A New Boundary Layer Mixing Scheme. Part I: Scheme Description and Single-Column Model Tests. *Monthly Weather Review*, 128(9), 3187–3199. https://doi.org/10.1175/1520-0493(2000)128<3187:ANBLMS>2.0.CO;2

Ludlam, F. (1967) Characteristics of billow clouds and their relation to clear-air turbulence. *Quarterly Journal of the Royal Meteorological Society*, 93(398), 419–435. https://doi.org/10.1002/qj.49709339803

Martins, L.D., Hallak, R., Alves, R.C., de Almeida, D.S., Squizzato, R., Moreira, C.A. et al. (2018) Long-range Transport of Aerosols from Biomass Burning over Southeastern South America and their Implications on Air Quality. *Aerosol and Air Quality Research*, 18(7), 1734–1745. Available from: https://doi.org/10.4209/aaqr.2017.11.0545

Mason, P. (1992) Large-eddy simulation of dispersion in convective boundary layers with wind shear. *Atmospheric Environment. Part A. General Topics*, 26(9), 1561–1571. https://www.sciencedirect.com/science/article/pii/096016869290056Q

McNider, R.T. & Pielke, R.A. (1981) Diurnal Boundary-Layer Development over Sloping Terrain. *Journal of Atmospheric Sciences*, 38(10), 2198–2212. Available from: https://doi.org/10.1175/1520-0469(1981)038%3C2198:DBLDOS%3E2.0.CO;2

Met Office. (2018) Monthly, seasonal and annual summaries 2018: July, Technical report, National Climate Information Centre, Met

Office, Exeter, UK. uk_monthly_climate_summary_201807.pdf. https://www.metoffice.gov.uk/research/climate/maps-and-data/summaries/index

Met Office. (2021) Monthly, seasonal and annual summaries 2021: April, Technical report, National Climate Information Centre, Met Office, Exeter, UK. uk_monthly_climate_summary_202104.pdf. https://www.metoffice.gov.uk/research/climate/maps-and-data/summaries/index

Milan, M., Macpherson, B., Tubbs, R., Dow, G., Inverarity, G., Mittermaier, M. et al. (2020) Hourly 4D-Var in the Met Office UKV operational forecast model. *Quarterly Journal of the Royal Meteorological Society*, 146(728), 1281–1301. https://rmets.onlinelibrary.wiley.com/doi/abs/10.1002/qj.3737

Miles, J.W. (1961) On the stability of heterogeneous shear flows. *Journal of Fluid Mechanics*, 10(4), 496–508. https://doi.org/10.1017/S0022112061000305

O'Doherty, S., Say, D., Stanley, K., Spain, G., Arnold, T., Rennick, C. et al. (2020) UK DECC (deriving emissions linked to climate change) network. In: *Centre for Environmental Data Analysis*. Harwell, UK: RAL Space Department, Science and Technology Facilities Council. http://catalogue.ceda.ac.uk/uuid/f5b38d1654d84b03ba79060746541e4f

Ott, S. & Ejsing Jørgensen, H. (2002) Meteorology and lidar data from the URAHFREP field trials, number 1212(EN) in 'Denmark. Forskningscenter Risoe. Risoe-R'. https://orbit.dtu.dk/en/publications/meteorology-and-lidar-data-from-the-urahfrep-field-trials

Prichard, B. (2018) July 2018 Mostly dry, warm and sunny; very warm in southeast. *Weather*, 73(9), i–iv. https://rmets.onlinelibrary.wiley.com/doi/abs/10.1002/wea.3143

Prichard, B. (2021) 'April 2021 Most places cold, sunny and very dry. *Weather*, 76(6), i–iv. https://rmets.onlinelibrary.wiley.com/doi/abs/10.1002/wea.4005

PubChem. (2023) National Center for Biotechnology Information. PubChem Element Summary for AtomicNumber 86, Radon. Tech. rep., U.S. National Library of Medicine. https://pubchem.ncbi.nlm.nih.gov/element/Radon.

Roach, W. (1970) On the influence of synoptic development on the production of high level turbulence. *Quarterly Journal of the Royal Meteorological Society*, 96(409), 413–429. https://doi.org/10.1002/qj.49709640906

Saito, K., Shimbori, T. & Draxler, R. (2015) JMA's regional atmospheric transport model calculations for the WMO technical task team on meteorological analyses for Fukushima Daiichi Nuclear Power Plant accident. *Journal of Environmental Radioactivity*, 139, 185–199. https://www.sciencedirect.com/science/article/pii/S0265931X14000563

Schepanski, K., Tegen, I., Todd, M.C., Heinold, B., Bönisch, G., Laurent, B. et al. (2009) Meteorological processes forcing Saharan dust emission inferred from MSG-SEVIRI observations of subdaily dust source activation and numerical mod. *Journal of Geophysical Research: Atmospheres*, 114(D10). https://agupubs.onlinelibrary.wiley.com/doi/abs/10.1029/2008JD010325

Schumann, U. (1996) Direct and large eddy simulations of stratified homogeneous shear flows. *Dynamics of Atmospheres and Oceans*, 23(1-4), 81–98. https://doi.org/10.1016/0377-0265(95)00423-8

Schwaiger, H.F., Denlinger, R.P. & Mastin, L.G. (2012) Ash3d: a finite-volume, conservative numerical model for ash transport and tephra deposition. *Journal of Geophysical Research: Solid Earth*, 117(B4). https://agupubs.onlinelibrary.wiley.com/doi/abs/10.1029/2011JB008968

Searcy, C., Dean, K. & Stringer, W. (1998) PUFF: A high-resolution volcanic ash tracking model. *Journal of Volcanology and Geothermal Research*, 80(1), 1–16. https://www.sciencedirect.com/science/article/pii/S0377027397000371

Sharman, R., Tebaldi, C., Wiener, G. & Wolff, J. (2006) An Integrated Approach to Mid- and Upper-Level Turbulence Forecasting An integrated approach to mid-and upper-level turbulence forecasting. *Weather and Forecasting*, 21(3), 268–287. https://doi.org/10.1175/WAF924.1

Sillman, S., Logan, J.A. & Wofsy, S.C. (1990) A regional scale model for ozone in the United States with subgrid representation of urban and power plant plumes. *Journal of Geophysical Research: Atmospheres*, 95(D5), 5731–5748. https://doi.org/10.1029/JD095iD05p05731

Stanley, K.M., Grant, A., O'Doherty, S., Young, D., Manning, A.J., Stavert, A.R. et al. (2018) Greenhouse gas measurements from a UK network of tall towers: technical description and first results. *Atmospheric Measurement Techniques*, 11(3), 1437–1458. https://doi.org/10.5194/amt-11-1437-2018

Stavert, A.R., O'Doherty, S., Stanley, K., Young, D., Manning, A.J., Lunt, M.F. et al. (2019) UK greenhouse gas measurements at two new tall towers for aiding emissions verification. *Atmospheric Measurement Techniques*, 12(8), 4495–4518. https://amt.copernicus.org/articles/12/4495/2019/

Stohl, A., Forster, C., Frank, A., Seibert, P. & Wotawa, G. (2005) Technical note: the lagrangian particle dispersion model FLEXPART version 6.2. *Atmospheric Chemistry and Physics*, 5(9), 2461–2474. https://acp.copernicus.org/articles/5/2461/2005/

Stull, R. (1999) *An Introduction to Boundary Layer Meteorology (Chapter1). Atmospheric and oceanographic sciences library*, 1st edition. Dordrecht, Netherlands: Kluwer Academic Publishers.

Stull, R. (2000) *Meteorology for Scientists and Engineers (Chapter 7)*, Earth Science Series, 2nd edition. Pacific Grove, CA: Brooks Cole.

Swallow, B., Rigby, M., Rougier, J., Manning, A., Lunt, M. & O'Doherty, S. (2017) Parametric uncertainty in complex environmental models: a cheap emulation approach for models with high-dimensional output, Technical report. https://www.researchgate.net/publication/313671187_Parametric_uncertainty_in_complex_environmental_models_a_cheap_emulation_approach_for_models_with_highdimensional_output

Thorpe, A.J. & Guymer, T.H. (1977) The nocturnal jet. *Quarterly Journal of the Royal Meteorological Society*, 103(438), 633–653. https://rmets.onlinelibrary.wiley.com/doi/abs/10.1002/qj.49710343809

Turner, D.B. (1997) The Long Lifetime of the Dispersion Methods of Pasquill in U.S. Regulatory Air Modeling. *Journal of Applied Meteorology*, 36(8), 1016–1020. https://journals.ametsoc.org/view/journals/apme/36/8/1520-0450_1997_036_1016_tllotd_2.0.co_2.xml

Van Der Laan, S., Karstens, U., Neubert, R., Van Der Laan-Luijkx, I. & Meijer, H. (2010) Observation-based estimates of fossil fuel-derived CO_2 emissions in the Netherlands using $\delta 14^C$, CO and ^{222}Radon. *Tellus B: Chemical and Physical*

Meteorology, 62(5), 389-402. https://doi.org/10.1111/j.1600-0889.2010.00493.x

Vinuesa, J.-F. & Galmarini, S. (2007) Characterization of the ^{222}Rn family turbulent transport in the convective atmospheric boundary layer. *Atmospheric Chemistry and Physics*, 7(3), 697–712. https://acp.copernicus.org/articles/7/697/2007/

Walters, D., Baran, A.J., Boutle, I., Brooks, M., Earnshaw, P., Edwards, J. et al. (2019) The Met Office Unified Model Global Atmosphere 7.0/7.1 and JULES Global Land 7.0 configurations. *Geoscientific Model Development*, 12(5), 1909–1963. https://doi.org/10.5194/gmd-12-1909-2019

Wei, W., Zhang, H., Zhang, X. & Che, H. (2023) Low-level Jets and Their Implications on Air Pollution: A Review. *Frontiers in Environmental Science*, 10, 88-95. https://www.frontiersin.org/articles/10.3389/fenvs.2022.1082623

SUPPORTING INFORMATION

Additional supporting information can be found online in the Supporting Information section at the end of this article.

How to cite this article: Mirza, A.K., Dacre, H.F. & Lo, C.H.B. (2024) A case study analysis of the impact of a new free tropospheric turbulence scheme on the dispersion of an atmospheric tracer. *Quarterly Journal of the Royal Meteorological Society*, 1–19. Available from: https://doi.org/10.1002/qj.4681